Sustainable Structures
ISSN: 2789-3111 (Print); ISSN: 2789-312X (Online)
http://www.sustain-dpl.com/journal/sust
DOI: 10.54113/j.sust.2025.000069

ORIGINAL ARTICLE

Seismic energy dissipation capacity of confined concrete columns with infilled-AAC bricks subjected to quasi-static cyclic loading

Bambang Sabariman[a], Tavio[b,*], Slamet Widodo[c]

[a]Department of Civil Engineering, Universitas Negeri Surabaya, Surabaya 60231, Indonesia
[b]Department of Civil Engineering, Institut Teknologi Sepuluh Nopember, Surabaya 60111, Indonesia
[c]Department of Civil Engineering, Universitas Negeri Yogyakarta, Yogyakarta 55281, Indonesia
[*]Corresponding Author: Tavio. Email: tavio@its.ac.id

Abstract: Autoclaved Aerated Concrete (AAC) is still designated as a non-engineering material because it is considered not to contribute to the stiffness and strength of structural members and is considered limited to infilling material within structural building frames. This provision needs to be reviewed because based on several studies its contribution to the stiffness and strength of the building structure is quite significant. This study involved tests of confined concrete column specimens infilled with AAC. The results indicate that its capability to dissipate the earthquake energy still satisfies all three criteria of the ACI 374.1-05 provisions, such as capability to carry loads > $0.75P_{h\text{-max}}$, relative energy dissipation ratio (β) > 0.125, and gradient hysteresis loop limited by drift ratio limit (-0.35% and +0.35) > 0.05. Apart from that, it is also able to enhance the column ductility to reach up to 9.285 (greater than 4), which is categorized as high ductility criteria in FEMA 356. All test columns in the study failed in flexural modes as designed (no shear failures occurred).

Keywords: Autoclaved aerated concrete, disaster risk reduction, ductility, seismic energy dissipation, stiffness, strength

1 Introduction

Building structures must be designed according to the conditions in which the building was built, particularly in earthquake-prone areas such as most areas in Indonesia. This design certainly requires innovation to improve the performance of the structure or structural members such as concrete beams or columns, especially since, in general, concrete is a construction material that has been used globally [1]. One innovation is to utilize lightweight bricks to strengthen column members [2], and the other one is to use masonry bricks made from red bricks and lightweight bricks to improve the concrete beam capacities [3]. This also considers that AAC as wall-filling can provide additional stiffness to structural elements [4-7]. Although several provisions [8, 9] define Autoclaved Aerated Concrete (AAC) only as a non-engineering material for building structures, which is considered no contribution to the stiffness and strength of structural members such as concrete beams and columns. However, on the other hand, other researchers [10] state that it still can provide a significant contribution to the strength of structural members.

The most rational way [11] to evaluate the capability of structural members is to apply the energy-based approach, namely seismic energy dissipation capacity. This energy is different from force or displacement. Energy is a scalar that can synthesize the effects of earthquakes on structures.

Received: 4 October 2024; Received in revised form: 4 February 2025; Accepted: 6 February 2025

Studying the behavior of reinforced concrete members that experience axial loading (columns) is a very important research topic for building structures in earthquake-prone areas, so it needs to be researched continuously. This also includes studying the shape and material of the columns which are expected to be able to dissipate earthquake energy well. It turns out that the energy dissipation also depends on the cross-sectional geometry, the axial load ratio, and the number of cycle repetitions that have a significant influence on the total energy dissipation [12].

Unfortunately, as far as the authors are concerned, not much research has been conducted on this topic which introduced AAC as a part of structural material cast in the midsection of concrete columns. The study particularly in terms of experimental investigation of their seismic behaviors is one of the major issues which required to be discovered. In this research, the middle of the column cross-section/geometry was filled with AAC with several thickness variations. This was carried out to investigate the seismic energy dissipation capacity of each variation.

2 Materials and Experimental Testing Procedure

2.1 Materials

The materials used in this research in columns filled with AAC include normal-strength concrete, longitudinal reinforcement, stirrups, and AAC. All of these materials were products from Indonesia. So that all the materials used in this research are reliable for future applications. Ready-mix concrete was also used in this research with the average f_c' = 40.78 MPa (standard deviation: 0.59 MPa). The properties of the materials used for steel reinforcement are D8 stirrups with the average f_{yh} = 446.82 MPa (standard deviation: 25.06 MPa) and ultimate elongation of 16.01% (standard deviation: 0.17%), D10 longitudinal steel bars with the average f_y = 445.11 MPa (standard deviation: 29.64 MPa) and ultimate elongation of 18.44% (standard deviation: 0.41%). The standard test methods and standard practice for concrete and steel bars used the common standards adopted in Indonesia, namely ASTM [13-15]. Each test involved three individual samples. The compressive strength of AAC is around 4.0 MPa. The materials used in the research have met the terms and conditions [16]. The reinforced concrete column specimens were prepared with and without infilling AAC. Column specimens without infilling AAC were designed according to SNI [17] with dimensions of 200 mm × 200 mm × 1000 mm as shown in **Fig. 1**, while column specimens with infilling AAC have their cross-sections divided into two equal areas (left and right) and in between were filled with AAC (see **Fig. 2** and **Tab. 1**).

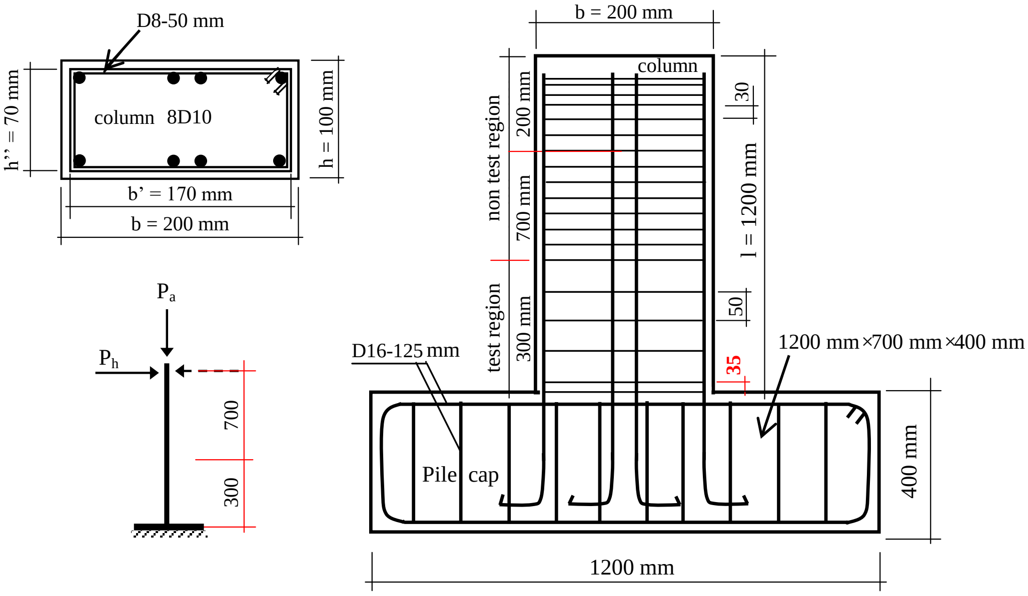

Fig. 1. Column without AAC.

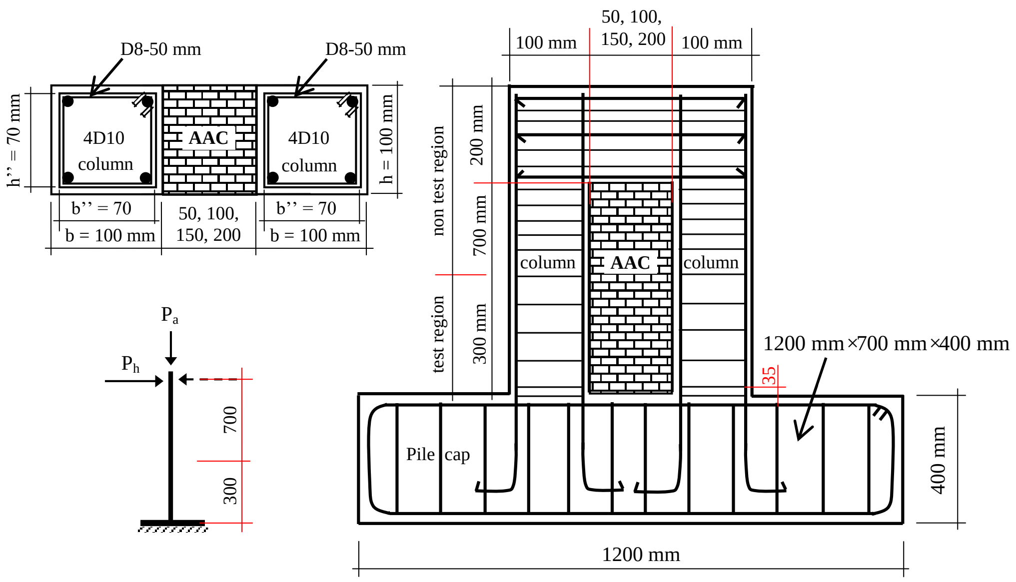

Fig. 2. Column with AAC (mm)

Table 1. Details of column test specimens

Column Specimen ID	Longitudinal Reinforcement	Transverse Reinforcement Spacing	AAC Brick Depth (mm)	Position of AAC
Column 1	8D10	D8-50	0	-
Column 2	8D10	D8-50	50	see **Fig.** 2
Column 3	8D10	D8-50	100	see **Fig.** 2
Column 4	8D10	D8-50	150	see **Fig.** 2
Column 5	8D10	D8-50	200	see **Fig.** 2

The ductilities of concrete members can be achieved by introducing steel fibers [18] or confinement using stirrups in concrete beams [19, 20] and steel fibers [21], welded reinforcement grids [22-25], fiber reinforced polymer [26], stirrups [27], spirals [28-31] and steel collars [32] in concrete columns under axial compression [18-21] and lateral reverse cyclic loading [33-36]. To provide adequate confinement, a confining value (Z_m) and the reinforcement and anchorage of the column test specimens are designed in such a way as to satisfy the requirements and provisions, along with the location of the AAC. The Z_m value is very important because it will affect the level of column ductility, the confining value Z_m [37] can be calculated based on the following equation:

$$Z_m = \frac{0.625}{\left[\dfrac{3+0.29 f'_c}{145. f'_c - 1000}\right] + \dfrac{3}{4}\rho_s \sqrt{\dfrac{b''}{s_h}} - 0.002K} \tag{1}$$

where Z_m is the modified Kent-Park concrete confinement value [37], $K = 1 + [(\rho_s \, . \, f_{yh}) / f_c']$, ρ_s is the volumetric ratio of stirrup reinforcement to confined concrete core measured from outer edge to outer edge of stirrups, s_h is the spacing from centerline/center to centerline/center of stirrups (mm), f_{yh} is the yield strength of stirrup reinforcement (MPa), f_c' is the compressive strength of concrete (MPa), and b'' is the cross-sectional dimension of confined concrete core measured from outer edge to outer edge of stirrups (mm).

The value of Z_m is very important in the arrangement of confinement. By knowing the value of Z_m, the value of s_h (stirrup spacing) can be found. Likewise, if the stirrup spacing is known, the value of Z_m can be determined. From the moment-ductility curve, a good arrangement of confinement can be achieved with a low value of Z_m. This can be determined by increasing the value of ρ_s. The greater the value of ρ_s, the better the confinement such that the value of Z_m is smaller, and thus, the smaller the value of Z_m, the better the ductility.

2.2 Experimental Test Procedure

All column specimens were tested with a displacement-controlled pattern following the protocol as shown in **Fig. 3.** Each test cycle was carried out three times in alternating phases based on ACI 374.1-05 [38]. This test began with a displacement of 0.2% drift ratio. The next cycle used a drift ratio of not less than 1.25 and not more than 1.5 times the previous drift ratio the increase in the drift ratio was carried out gradually until a minimum drift ratio value of 0.035 or 3.5% was achieved. A drift ratio of 3.5% can also be called a normal condition for testing the achievement of ductility for column specimens tested with quasi-cyclic loading. However, in this study, the new cycle was stopped after the test specimen collapsed, which was around the 15th cycle, the cycle in question is listed in **Tab**. **2.**

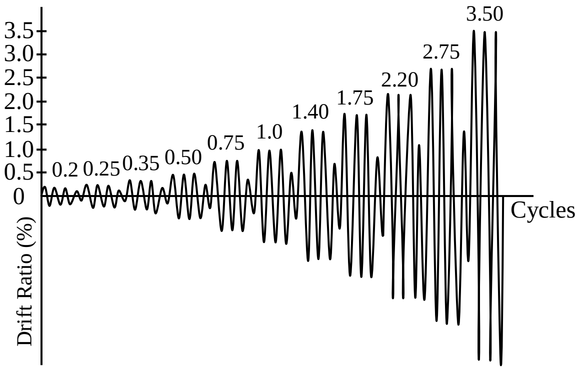

Fig. 3. Displacement controlled cycles [38].

Table 2. Drift ratio for all column specimens, L_{col} = 1000 mm

Cycle	Drift ratio (%)	Lateral displacement (mm)
1	0.20	2.00
2	0.25	2.50
3	0.35	3.50
4	0.50	5.00
5	0.75	7.50
6	1.00	10.00
7	1.40	14.00
8	1.75	17.50
9	2.20	22.00
10	2.75	27.50
11	3.50	35.00
12	4.38	43.75
13	5.47	54.69
14	6.84	68.36
15	8.54	85.45
16	10.68	106.81
17	13.35	133.51

2.3 Criteria and Energy Dissipation Calculation

Criterion 1: The load that can be carried must be greater than 75% of the maximum load (see **Fig. 4(a)**). Criterion 2: The comparison value between the area formed by the hysteretic loop and the area of the parallelogram formed from the intersection of the ends of the hysteretic loop at story drift 3.50% of the 3rd cycle with the stiffness at story drift 0.2% of the 1st cycle must be greater than 0.125 (see **Fig. 4(b)**). Criterion 3: The comparison value of the gradient of the hysteresis loop limited by -0.35% and +0.35% must be greater than or equal to 0.05 times the initial gradient value of the structural module at the 1st loading cycle (see **Fig. 4(c)**).

The magnitude of energy dissipation can be calculated from the shaded area in **Fig. 4(b)**. The K and K' values are taken based on the slope of the drift ratio value of 0.2% in the 1st cycle of the 3rd

phase [38], while the drift ratio at 3.5% in the third phase is the maximum drift for calculating energy dissipation. Therefore, testing at a drift ratio of 0.2% must be carried out carefully and cautiously, because it will determine two parallelograms, namely parallelograms ABCD and DFGA (see **Fig. 4(b)**) as well as the basis for calculating column energy dissipation.

The experimental data from this research were all converted to a daTabase. It is in the form of thousands of data with X and Y coordinates. For instance, data X_i, X_{i+1}, and Y_i, Y_{i+1} is taken, then the dissipation area Z_{i+1} can be calculated using the following equation:

$$\text{Dissipation area} \quad Z_{i+1} = \frac{(X_{i+1} - X_i) \times (Y_{i+1} + Y_i)}{2} \tag{2}$$

According to ACI 374.1-05 [38], the conditions that need to be explained/anticipated are that for specimens tested with cyclic loads, it is required that they do not experience strength degradation, where this condition can occur if the peak force value (P_h) on the specimen is less than 75% of the maximum lateral load value (E_{max}). This condition will affect the steepness of the drift value and the load after the peak force.

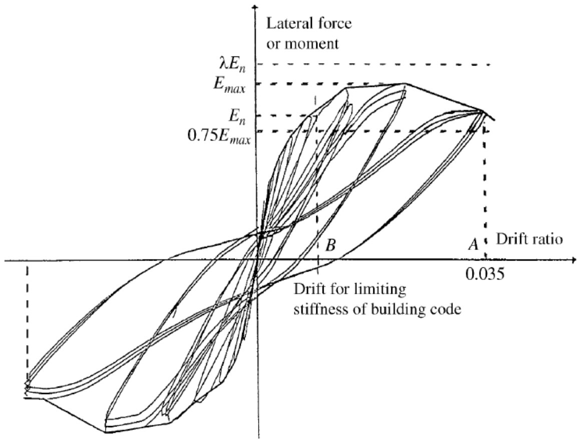

(a) Quantities used in evaluating acceptance criteria

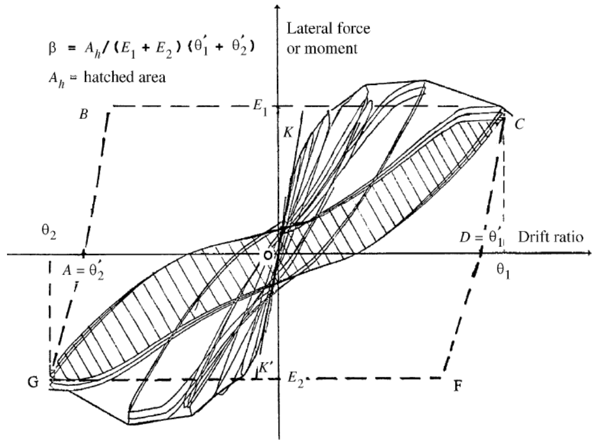

(b) Shaded area represents the relative energy dissipation ratio of the two parallelograms, ABCD and DFGA

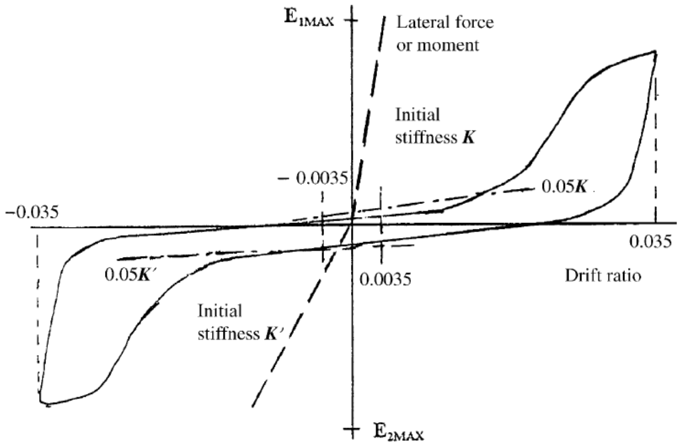

(c) Unacceptable hysteretic behavior

Fig. 4. Criteria according to ACI 374.1-05 [38].

2.4 Column Ductility

Based on FEMA 356 Tab. 6.6 [39], the displacement ductility criteria are:

(1) Low ductility demand: $\mu_\Delta < 2$

(2) Moderate ductility demand: $2 \leq \mu_\Delta \leq 4$

(3) High ductility demand: $\mu_\Delta > 4$

The displacement ductility value is obtained using the equation:

$$\mu_\Delta = \Delta_u / \Delta_y \tag{3}$$

Determination of the 1st yield point can be measured based on the measurement results from the strain gauge installed on the main reinforcement, but some researchers practically define this point based on **Fig. 5.**

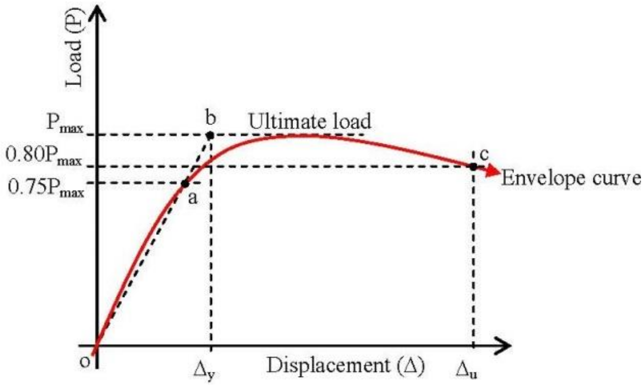

Fig. 5. Definition of yield displacement [40,41].

Fig. 6. Actual test setup and drift that occurred during testing.

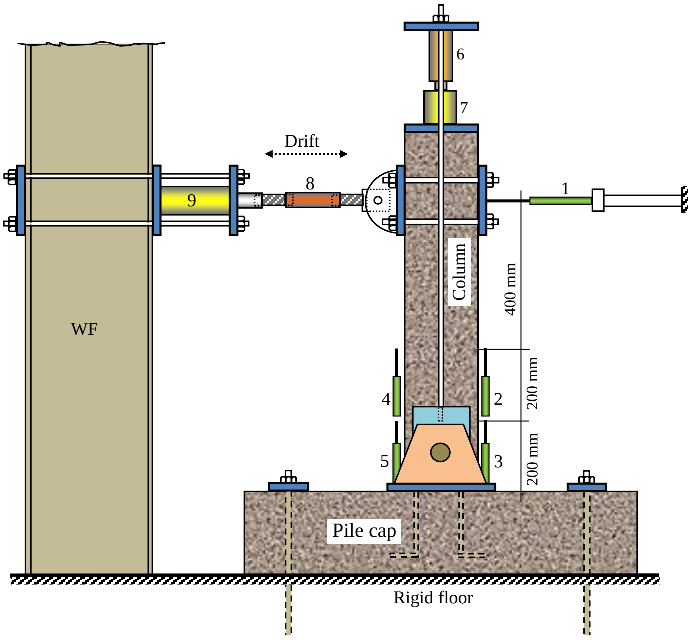

Fig. 7. Schematic test setup [44-46] adapted to the laboratory conditions, 1-5 = LVDT (linear variable displacement transducer), 6 = single-acting hydraulic jack, 7 = single-acting load cell, 8 = double-acting load cell, 9 = double-acting hydraulic jack, = quasi-cyclic load direction.

The quasi-cyclic test result data from phase 0 to the final phase (the condition of the test specimen has collapsed) is depicted in a 2D curve, then the envelope curve is depicted from this image, and the value of the 1st displacement yielding point Δ_y can be practically determined. Determination of the 1st displacement yielding point Δ_y can be obtained by drawing a horizontal line $0.75P_{h\text{-}max}$ to the right intersecting the envelope curve to obtain Point a. Then draw a straight line oa intersecting the horizontal line $P_{h\text{-}max}$ to obtain Point b. Thereafter, draw a vertical line down to obtain the value of Δ_y, while the ultimate displacement value is based on a decrease in strength of 20%, namely $0.80P_{h\text{-}max}$ [42]. The method is to draw a line from $0.80P_{h\text{-}max}$ to the right and intersect the envelope curve line to find Point b, from Point b then draw a vertical line down to obtain the displacement limit value (ultimate displacement-Δ_u).

In addition, drift (Δ) can be understood in general as a function of several parameters and can be simplified that Δ = f(load, element length, moment, elastic modulus, and moment of inertia) [43], meaning that in this case, the existing structural cross-section can have its moment of inertia (I) value increased without changing the area and size of the cross-section. The moment is $P_h.L$, so that due to changes in the inertia of the cross-section there will be changes in the magnitude of deflection and P_h.

2.5 Quasi-Cyclic Test Setup

Measurement data related to energy capacity and column ductility are attempted to be recorded as well as possible. This aims to ensure that data processing and analysis are sufficient to support the validity of the analysis of energy capacity and column ductility. Therefore, a representative test setup is required according to the loading protocol [38] as shown in **Figs. 6** and **7.**

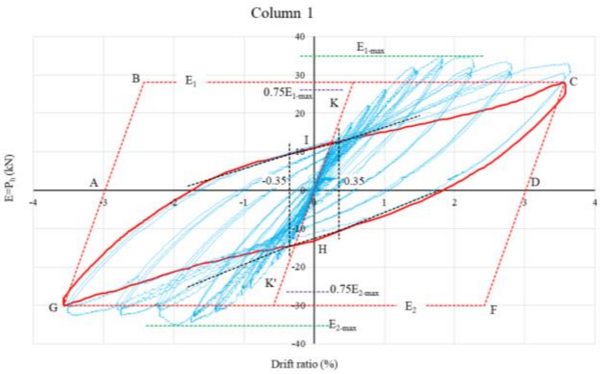

(a) Column 1

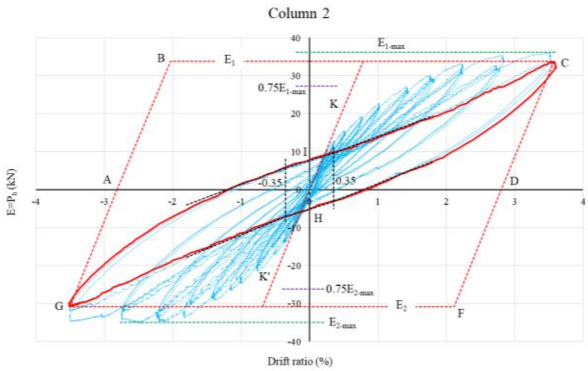

(b) Column 2

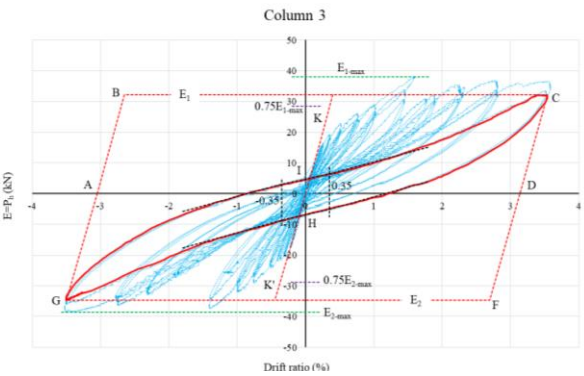

(c) Column 3

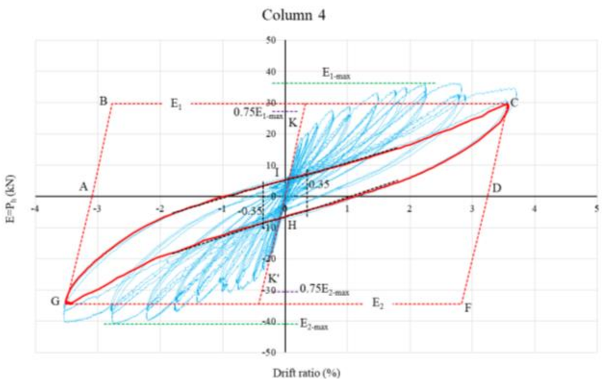

(d) Column 4

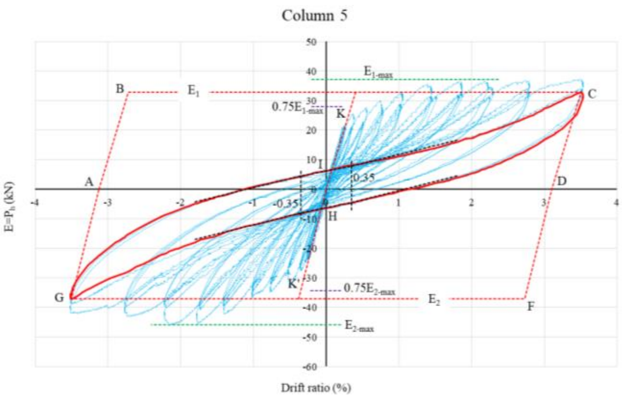

(e) Column 5

Fig. 8. Relative energy dissipations.

3 Results and Discussion

3.1 Seismic Energy Dissipation Measurement of Column Specimens

Energy dissipation measurements are adjusted to the ACI 374.1-05 [38] criteria, which is based on the drift ratio at conditions of 0%–3.5%. Thus, the drift ratio > 3.5% is not depicted. Therefore, this measurement data only shows the relationship between the drift ratio of 0% to 3.5% vs. lateral load (P_h), and the story drift of 3.5% is taken in the 3rd cycle which is represented by the red line hysteretic loop, while the drift ratio of 0%–3.5% in the 2nd phase is represented by the blue strip lines. The results can be seen in **Fig. 8.**

Based on **Fig. 8**, the relative dissipation energy can be calculated in the form of an area (abscissa times ordinate) limited by the red line CHGI, but in this case, the drift ratio value in percent units is converted back into a drift value in mm units, such that the multiplication of the abscissa and ordinate in kN.mm units can be obtained. The ideal energy dissipation area is limited by the dashed red line or in the form of the area of two parallelograms ABCD and DFGA. The condition for the acceptance of the relative dissipation energy in this study is controlled by a drift of no less than a drift ratio of 3.5% in the 3rd phase must meet three criteria (see Section 2.3).

The calculation results as the basis for the acceptance of the three criteria [38] are as follows in **Tab**. **3.**

Table 3. Capability to withstand lateral forces as the fulfillment of Criterion 1

Specimen ID	$0.75P_{h\text{-}max}$ (kN)		$P_{h\text{-}3.5\%} > 0.75P_{h\text{-}max}$ (kN)	
	Compression	Tension	Compression	Tension
Column 1	26.440	26.166	30.038	28.075
Column 2	26.214	27.177	30.799	33.747
Column 3	28.925	28.497	34.698	32.179
Column 4	30.672	27.201	34.508	29.563
Column 5	34.429	27.866	37.092	32.939

Table 4. Relative energy dissipation ratio (β) as the fulfillment of Criterion 2

Specimen ID	Area of ABCD and DFGA (kN.mm)	Area of CHGI (kN.mm)	β of each column
Column 1	3482.811	1243.236	0.357 > 0.125
Column 2	3624.798	758.190	0.209 > 0.125
Column 3	4357.093	744.206	0.171 > 0.125
Column 4	4143.939	746.526	0.180 > 0.125
Column 5	4469.651	824.845	0.185 > 0.125

Table 5. Gradient hysteresis loop limited by drift ratio limit -0.35% and +0.35, as the fulfillment of Criterion 3

Specimen ID	Gradient of hysteresis loop		
	Compression	Tension	Average
Column 1	0.113 > 0.05	0.090 > 0.05	0.102 > 0.05
Column 2	0.132 > 0.05	0.125 > 0.05	0.128 > 0.05
Column 3	0.065 > 0.05	0.060 > 0.05	0.062 > 0.05
Column 4	0.066 > 0.05	0.053 > 0.05	0.059 > 0.05
Column 5	0.051 > 0.05	0.060 > 0.05	0.055 > 0.05

Table 6. Comparison of the values of each β to β of Column 1

Specimen ID	Area of ABCD and DFGA (kN.mm)	Area of CHGI (kN.mm)	β of each column
Column 1	3482.811	1243.236	0.357 > 0.125
Column 2	-	758.190	0.218 > 0.125
Column 3	-	744.206	0.2317 > 0.125
Column 4	-	746.526	0.2143 > 0.125
Column 5	-	824.845	0.237 > 0.125

Based on **Tab**s. **3 to 5**, all test specimens have satisfied the requirements of the three criteria [38].

In addition, if Column 1 is considered as a benchmark for acceptance for all test specimens, then it is still actually seen that the β value is > 0.125 for all test specimens (see **Tab**. **6**). However, the increase of the AAC size in Column 5 by 200 mm, or the same as the initial size of Column 1 is considered to be the maximum. This can be seen from the gradient hysteresis loop value which is approaching the value of 0.05.

3.2 Column Ductility

The envelope curve of the hysteresis loop shown here is the relationship between P_h (kN) and drift ratio (%) [47] starting from 0% until the column collapses according to **Tab**. **2.** This is expected to be able to gain an idea of the value of $0.8P_{h\text{-}max}$ (a decrease in strength of 20%) after the peak load [42]. This must be carried out as the basis for calculating the ductility of the column. The results are given in **Fig. 9.**

3.3 Lateral Force (P_h)

Based on the design where an attempt is made to increase the moment of inertia of the column, due to the presence of the infilling AAC, **Tab**. **7** displays the data of the magnitude of P_h according to the changes in cross-section.

The capability of the column to absorb seismic energy is represented in **Fig. 9** (red line CHGI) and **Tab**s. **7** and **8**, where the size can be calculated as the area of CHGI by multiplying the abscissa times the ordinate [48]. The result of the multiplication is the capability to dissipate seismic energy. This energy can counteract earthquake force, and can also be used as a mainstay to support the safety of the structural column, such that the safety of dwellers of the building can be assured.

Table 7. Column lateral force

Specimen ID	Lateral force $P_{h\text{-}max}$ (kN)		
	Compression	Tension	Average
Column 1	35.253	34.889	35.071
Column 2	34.952	36.236	35.594
Column 3	38.566	37.995	38.281
Column 4	40.896	36.268	38.582
Column 5	45.905	37.155	41.530

Table 8. Column ductility

Specimen ID	Gradient of hysteresis loop			Criteria according to FEMA [39]
	Compression	Tension	Average	
Column 1	5.742	5.304	5.523 > 4	High ductility
Column 2	4.672	3.763	4.218 > 4	High ductility
Column 3	7.231	5,224	6.228 > 4	High ductility
Column 4	6.731	7.430	7.080 > 4	High ductility
Column 5	9.088	9.482	9.285 > 4	High ductility

The size of the CHGI area can vary because it depends on the height of P_h (kN) times the length of the drift (mm). In certain cases with several areas that are almost the same, it can come from different P_h and drift, it can be a high $P_{h\text{-}max}$ or a large drift, a larger drift is more beneficial in its effect on column ductility.

In this study, the areas of CHGI of Columns 2 to 5 indicate that the energy dissipation areas are almost the same as each other, but the drift values are more varied and larger than the drift of Column 1. This causes a greater ductility value, if the displacement value at the 1st yield is small, then this ductility value is even smaller. The smaller the first yield displacement value indicates that the column is getting stiffer. This stiffness is also caused by the concrete restraint (Z_m). In this case, the confinement of the column without AAC is represented by the X and Y stirrups which are all two-legged, whereas in columns with AAC, the X stirrups are four-legged and the Y stirrups are two-legged. Thus, in this case, they cause the Z_m confinement value to be smaller. The smaller the Z_m value, the more ductile the column is.

The moment of inertia due to the separation of the column which was filled with the AAC between the columns, also caused an increase in the moment of inertia. This indirectly also affected the increase in the lateral force resisted by the columns (see **Tab. 7**) and the capability of the column to perform a more ductile displacement beyond its inelasticity (see **Tab. 8**).

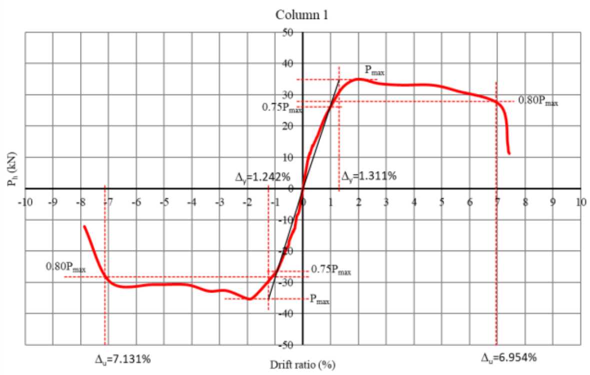

(a) Column 1

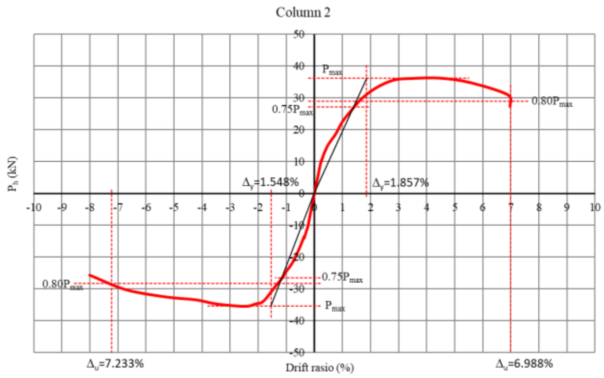

(b) Column 2

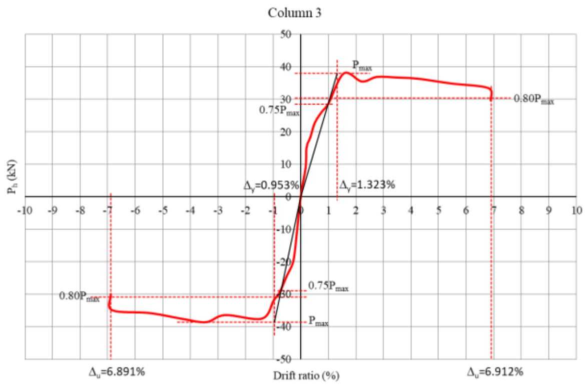

(c) Column 3

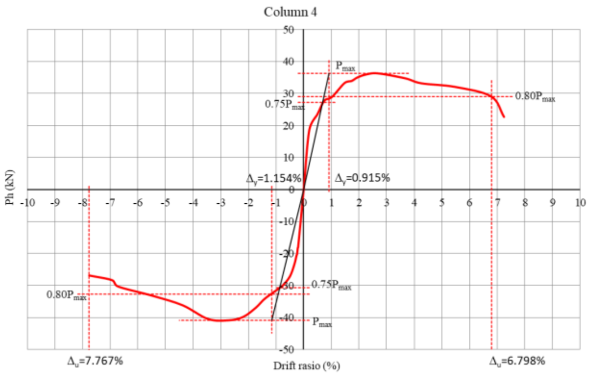

(d) Column 4

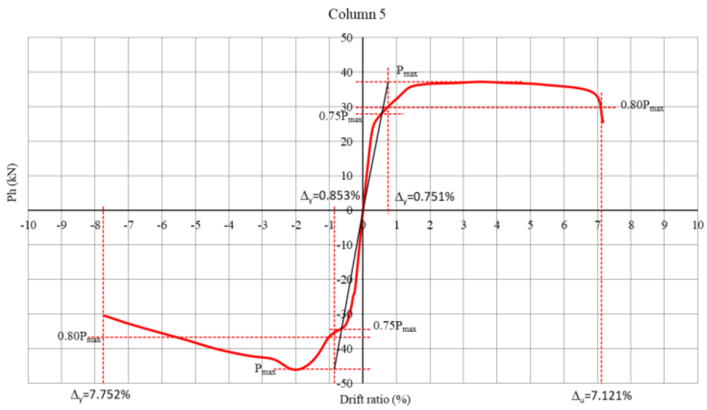

(e) Column 5

Fig. 9. Envelope curves from hysteresis loops.

3.4 Cracking of Column Specimens

Based on the initial design, flexural failures are expected to occur in the column specimens. The results indicated that all test specimens experienced flexural failures, where the damage concentrations were not too long. The crack path also looks horizontal (characteristic of flexural cracks) not oblique cracks (characteristic of shear cracks). The length of the damage also tends to be short, around 100 to 150 mm, meaning that the length of this plastic hinge is influenced by the flexural force. The appearance of cracks in each test specimen is shown in **Fig. 10.**

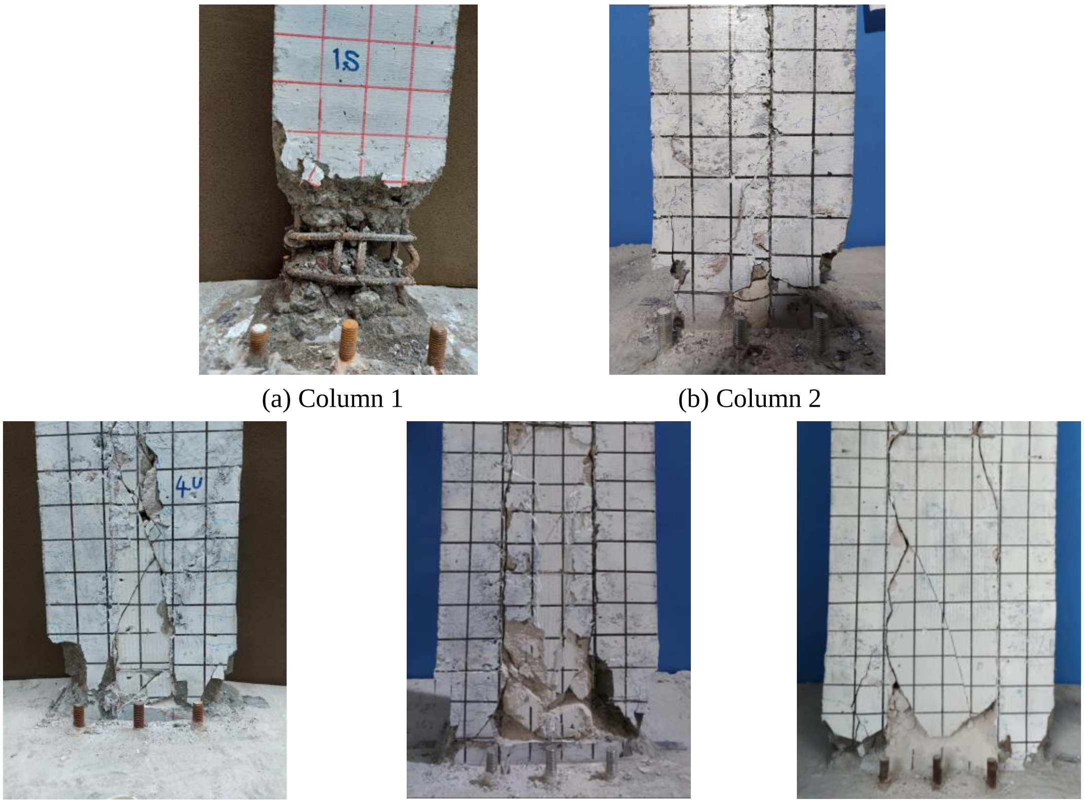

(a) Column 1 (b) Column 2

(c) Column 3 (d) Column 4 (e) Column 5

Fig. 10. Column cracks and plastic hinges occurred in the range of 100 to 150 mm.

4 Conclusions

Basically, the capability to dissipate seismic energy aims to serve as a guarantee of safety for dwellers of buildings, namely when the structure has decreased in strength after peak loads. This guarantee has been governed in ACI 374.1-05 in three criteria. This study proposed the use of AAC as infilling material in column cross sections. Several AAC sizes have been introduced in the study. The results indicate that most have satisfied the three criteria. Even in this study, energy dissipation was also compared to the ideal energy dissipation of Column 1 (area of Column 1 tier row), the results of all test specimens still satisfied the acceptance requirements. To strengthen the results of this study, the ductilities of all column specimens were observed and it turned out that all test specimens had reached high ductilities. Thus, this ductility achievement has strengthened the acceptance requirements of the column specimens.

This study limits the size of the AAC to be the same as the initial size of the column cross-section, which is 200 mm. This is limited such that the column does not behave as an infilling AAC wall in the concrete frame since the column in this study has been designed to fail in a flexural manner. All test column specimens failed in flexure (none has failed in shear).

Acknowledgment

The authors gratefully acknowledge financial support from the Institut Teknologi Sepuluh Nopember for this work, under the Capacity Development Program of Higher Education for Technology and Innovation Project Asian Development Bank Loan No 4110-INO. The authors also express their sincere gratitude for all the funding received from the 2024 Indonesian Collaborative Research Grant, under UNESA with contract no. B/43867/UN38.III.1/LK.04.00/2024, and UNY with contract no. T/18.1.13/UN34.9/PT.01.03/2024. The authors gratefully acknowledge the financial support received from the Institut Teknologi Sepuluh Nopember for this work, under the project scheme of the Publication Writing and IPR Incentive Program (PPHKI) 2024.

Credit authorship contribution statement

Bambang Sabariman: Investigation, Writing–original draft. **Tavio**: Conceptualization, Supervision, Writing–review & editing. **Slamet Widodo**: Experimental preparation & testing, Analysis.

Conflicts of Interest

The authors declare that they have no conflicts of interest to report regarding the present study.

References

[1] He CH, Liu HW, Liu C. Fractal-based approach to the mechanical properties of recycled aggregate concretes. Facta Universitatis Series: Mechanical Engineering 2024; 22(2): 329-342. https://doi.org/10.22190/FUME240605035H.

[2] Tavio, Sabariman B. Contribution of lightweight brick infiller on strength and stiffness of RC columns under cyclic loading. International Journal on Engineering Applications 2022; 10(5): 384-392. https://doi.org/10.15866/irea.v10i5.20457.

[3] Tavio, Sabariman B. Behavior of masonry-infilled concrete beams. AIP Conference Proceedings 2023; 2629(040010): 1-8. https://doi.org/10.1063/5.0128852.

[4] Wijaya H, Rajeev P, Gad E, Amirsardari A. Effect of infill-wall material types and modeling techniques on the seismic response of reinforced concrete buildings. ASCE Natural Hazards Review 2020; 21(3): 1-15. https://doi.org/10.1061/(ASCE)NH.1527-6996.0000395.

[5] Fenerci A. The effect of infill walls on the seismic performance of boundary columns in reinforced concrete frames. Thesis of Graduate School of Natural and Applied Sciences of Middle East Technical University, 2013. Available: https://etd.lib.metu.edu.tr/upload/12616436/index.pdf.

[6] Qian K, Li B. Effects of masonry infill wall on the performance of RC frames to resist progressive collapse. ASCE Journal of Structural Engineering 2017; 143(9): 1-17. https://doi.org/10.1061/(ASCE)ST.1943-541X.0001860.

[7] Moretti ML, Papatheocharis T, Perdikaris PC. Design of reinforced concrete infilled frames. ASCE Journal of Structural Engineering 2014; 140(9): 1-10. https://doi.org/10.1061/(ASCE)ST.1943-541X.0001042.

[8] ACI Committee 319, Building code requirements for structural concrete and commentary (ACI 318-19). American Concrete Institute, USA, 2019.

[9] SNI Committee, Standard of seismic resistance design for building structures (SNI 1726:2019). National Standardization Board (in Indonesian), 2019.

[10] Pradeep S. Behavior of reinforced concrete frame with short column effect under lateral cyclic loading. Asian Journal of Civil Engineering 2017; 18(6): 879-891. Available: https://www.researchgate.net/publication/334625676.

[11] Galé-Lamuela D, Donaire-Avila J, Escolano-Margarit D, González-Sanz G, Benavent-Climent A. Energy dissipation capacity of RC columns subjected to unidirectional and bidirectional seismic loading. COMPDYN 2019: 7th ECCOMAS Thematic Conference on Computational Methods in Structural Dynamics and Earthquake Engineering 2019; https://doi.org/10.7712/120119.7078.19108.

[12] Rodrigues H, Arêde A, Varum H, Costa AG. Energy dissipation and equivalent damping of RC columns subjected to biaxial bending: an investigation based on experimental results. 15th World Conference on Earthquake Engineering (WCEE) 2012. Available: https://www.iitk.ac.in/nicee/wcee/article/WCEE2012_4127.pdf.

[13] ASTM Subcommittee: C09.61. Standard Test Method for Compressive Strength of Cylindrical Concrete Specimens (ASTM C39/C39M-24); American Society of Testing and Materials 2024; 04.02: 8. https://doi.org/10.1520/C0039_C0039M-24.

[14] ASTM Subcommittee: C09.61. Standard Practice for Making and Curing Concrete Test Specimens in the Laboratory (C192/C192M-24); American Society of Testing and Materials 2024; 04.02: 8. https://doi.org/10.1520/C0192_C0192M-24.

[15] ASTM Subcommittee: A01.13. Standard Test Methods and Definitions for Mechanical Testing of Steel Products (ASTM A370-24a); American Society of Testing and Materials 2024; 01.01, 01.02, 01.03, 01.04, 01.05: 51. https://doi.org/10.1520/A0370-24A.

[16] SNI Committee, Concrete reinforcing steel (SNI 2052:2017). National Standardization Board (in Indonesian), 2017.

[17] SNI Committee, Structural concrete requirements for buildings (SNI 2847:2019). National Standardization Board (in Indonesian), 2019.

[18] Christianto D, Kurniadi, D. Effect of steel fiber on the shear strength of reactive powder concrete. IOP Conference Series: Materials Science and Engineering 2019; 508(012006): 1-10. https://doi.org/10.1088/17

57-899x/508/1/012006.
[19] Anggraini R, Raka IGP. Flexural capacity of concrete beams reinforced with high-strength steel bars under monotonic loading. International Journal of GEOMATE 2021; 20(77): 173-180. https://doi.org/10.21660/2020.77.j2005.
[20] Anggraini R, Raka IGP, Agustiar. Experimental load-drift relations of concrete beam reinforced and confined with high-strength steel bars under reversed cyclic loading. ASEAN Engineering Journal 2021; 11(4): 56-69. https://doi.org/10.11113/aej.v11.17864.
[21] Sabariman B, Soehardjono A, Wisnumurti, Wibowo A. Stress-strain model for confined fiber-reinforced concrete under axial compression. Archives of Civil Engineering 2020; 66(2): 119-133. https:// doi.org/10.24425/ace.2020.131800.
[22] Tavio, Kusuma B. Experimental behavior of concrete columns confined by welded wire fabric as transverse reinforcement under axial compression. ACI Structural Journal 2012; 109(3): 339-348. https://doi.org/10.14359/51683747.
[23] Kusuma B, Tavio. Axial load behavior of concrete columns with welded wire fabric as transverse reinforcement. Elsevier: Procedia Engineering Journal 2011; 14: 2039-2047. https://doi.org/10.1016/j.proeng.2011.07.256.
[24] Tavio, Kusuma B. Investigation of stress-strain models for confinement of concrete by welded wire fabric. Elsevier: Procedia Engineering Journal 2011; 14: 2031-2038. https://doi.org/10.1016/j.proeng.2011.07.255.
[25] Tavio, Kusuma B. Stress-strain model for high-strength concrete confined by welded wire fabric. ASCE: Journal of Materials in Civil Engineering 2009; 21(1): 40-45. https://doi.org/10.1061/(asce)0899-1561(2009)21:1(40).
[26] Pinto D, Raka IGP. Axial compressive behavior of square concrete columns retrofitted with GFRP straps. International Journal of Civil Engineering and Technology 2019; 10(1): 2388-2400. Available: https://www.researchgate.net/publication/331271577.
[27] Agustiar, Raka IGP, Anggraini R. Behavior of concrete columns reinforced and confined by high-strength steel bars. International Journal of Civil Engineering and Technology 2018; 9(7): 1249-1257. Available: https://www.researchgate.net/publication/327335266.
[28] Machmoed SP, Raka IGP. Potential of new innovative confinement for square reinforced concrete columns. IOP Journal of Physics: Conference Series 2020; 1469(012027): 1-7. https://doi.org/10.1088/1742-6596/1469/1/012027.
[29] Sabariman B, Soehardjono A, Wisnumurti, Wibowo A. Stress-strain behavior of steel fiber-reinforced concrete cylinders spirally confined with steel bars. Advances in Civil Engineering, 2018; 6940532: 1-8. https://doi.org/10.1155/2018/6940532.
[30] Tavio, Machmoed SP, Raka IGP. Behavior of square RC columns confined with interlocking square spiral under axial compressive loading. International Journal on Engineering Applications 2022; 10(5): 322-335. https://doi.org/10.15866/irea.v10i5.20655.
[31] Machmoed SP, Raka IGP. Performance of square reinforced concrete columns confined with innovative confining system under axial compression. International Journal of GEOMATE 2021; 21(85): 137-144. https://doi.org/10.21660/2021.85.j2085.
[32] Pudjisuryadi P, Tavio, Suprobo P. Axial compressive behavior of square concrete columns externally collared by light structural steel angle sections. International Journal of Applied Engineering Research 2016; 11(7): 4655-4666. Available: https://www.researchgate.net/publication/303369333.
[33] Tavio, Kusuma B. Ductility of confined reinforced concrete columns with welded reinforcement grids. Excellence in Concrete Construction through Innovation–Proceedings of the International Conference on Concrete Construction 2008; 339-344. https://doi.org/10.1201/9780203883440.ch51.
[34] Tavio, Kusuma B. Strength and ductility enhancement of reinforced HSC columns confined with high-strength transverse steel. Proceedings of the Eleventh East Asia-Pacific Conference on Structural Engineering and Construction (EASEC-11) 2008; 350-351. Available: https://www.researchgate.net/publication/289034283.
[35] Pudjisuryadi P, Tavio. Performance of square reinforced concrete columns externally confined by steel angle collars under combined axial and lateral load. Elsevier: Procedia Engineering 2015; 125: 1043-1049. https://doi.org/10.1016/j.proeng.2015.11.160.
[36] Soehardjono A, Sabariman B, Wisnumurti, Wibowo A. Contribution of steel fibers on ductility of confined concrete columns. International Journal of GEOMATE 2022; 23(97): 188-195. https://doi.org/10.21660/2022.97.3483.
[37] Scott BD, Park R, Priestley MJN. Stress-strain behavior of concrete confined by overlapping hoops at low and high strain rates. Journal of American Concrete Institute 1982; 79: 13-27. https://doi.org/10.14359/10875.
[38] ACI Committee 374. Acceptance criteria for moment frames based on structural testing and commentary (ACI 374.1-05). American Concrete Institute, USA, 2014.

[39] FEMA 356. Prestandard and commentary for the seismic rehabilitation of buildings. Federal Emergency Management Agency, USA, 2000.

[40] Brachmann I, Browning JA, Matamoros A. Drift-dependent confinement requirements for reinforced concrete columns under cyclic loading. ACI Structural Journal 2004; 101(5): 669-677. https://doi.or g/10.14359/13389.

[41] Park R. State-of-the-art report: ductility evaluation from laboratory and analytical testing. Proceedings of Ninth World Conference on Earthquake Engineering 1988; VIII: 605-616. Available: https://www.iitk.ac.in/nicee/wcee/article/9_vol8_605.pdf.

[42] Elwood KJ, Maffei JM, Riederer KA, Telleen K. Improving column confinement—part 2: proposed new provisions for the ACI 318 building code. Concrete International 2009; 31(12): 41-48. Available: https://www.researchgate.net/publication/290482874.

[43] McCormac JC, Brown RH. Design of reinforced concrete. Ninth edition, John Wiley & Sons, USA, 2005.

[44] Tavio, Sabariman B, Widodo S. Effect of steel fiber on plastic hinge length of concrete columns: Buckingham theory application. Civil Engineering Journal 2024; 10(5): 1386-1408. https://doi.org/10.28991/cej-2024-010-05-03.

[45] Widodo S, Sabariman B, Tavio. Parametric study on contribution of combined confining steel and steel fiber to column's displacement ductility. Engineering and Applied Science Research 2024; 51(4): 473-481. http://doi.org/10.14456/easr.2024.44.

[46] Sabariman B, Tavio, Widodo S. Effect of steel fiber and confinement on capacities of RC columns in dissipating seismic energy. International Review of Civil Engineering 2024; 15(3): 287-296. https://doi.or g/10.15866/irece.v15i3.24513.

[47] Wang W, Wang J, Guo L. Mechanical behavior analysis of LEM-infilled cold-formed steel walls. Sustainable Structures 2022; 2(1): 000013. http://doi.org/10.54113/j.sust.2022.000013.

[48] Brown P, Evans M, Hunt D, McIntosh J, Pender B, Ramagge J. Introduction to coordinate geometry: a guide for teachers-years 9–10. Number and Algebra 2011; Module 29, the University of Melbourne, June 2011. Available: https://amsi.org.au/teacher_modules/pdfs/Introduction_to_coordinate_geometry.pdf.